INFLUENCE OF DEFECTS ON THE STRUCTURE OF OXYGEN PRECIPITATES IN SILICON CRYSTALS

V.G. LITOVCHENKO, I.P. LISOVS'KYY, V.P. KLAD'KO, S.O. ZLOBIN, M.V. MURAVS'KA, A.A. EFREMOV, M.V. SLOBODYAN

V.E. Lashkarev Institute of Semiconductor Physics, Nat. Acad. Sci. of Ukraine
(41, Nauky Prosp., Kyiv 03680, Ukraine)

UDC 621.315.592.3
©2007

The methods of IR-spectroscopy with the computer analysis of the absorption band form, electron microscopy, and X-ray diffraction and measurements of a decrease of the nonstationary photoconduction under conditions of a low excitation level were used for the experimental investigation of the influence of defects in silicon ingots of various diameters (40–300 mm) on the processes of formation of oxygen precipitates due to the two-stage annealing (750 and 1050 °C). The investigations were performed for silicon monocrystals grown by the Czochralski method (Cz-Si). It is shown that large-diameter samples include electrically active microdefects of a relatively low concentration which are small (0.06—0.1 μm) dislocation loops. Due to this fact, a weakly stressed phase of SiO_2 oxide, which doesn't contain the deformed 4-membered rings of SiO_4 tetrahedra (characteristic of the precipitated silicon-oxygen phase in low-diameter ingots), is formed in the process of thermal treatments. As a result, a higher thermostability of such a silicon is observed.

1. Introduction

The properties and behavior of oxygen complexes in Cz-Si materials is important for various stages of the modern microelectronic technology. In this connection, they were investigated in many works (see, e.g., [1–4]). However, for large-diameter samples produced with the help of a number of up-to-date technological techniques with additional doping (e.g., by nitrogen), this problem isn't sufficiently investigated. The improvement of the Cz-Si growth technology related to an increase in the diameter of samples can influence the behavior of this material during the following thermal treatments that, in particular, results in creation of oxygen precipitates (precipitation of the SiO_2 dielectric phase). An important role in this process is played by the defect-structural state of a crystal. This fact has conditioned the problem statement of the given work devoted to the comparative investigation of the structural state of oxygen in Cz-Si ingots of various diameters and its variation due to thermal treatments.

2. Experimental Technique

We investigated Cz-Si plates 0.4–0.9 mm in thickness with (100) orientation of the surface that had been cut out of ingots 40–300 mm in diameter and polished on both sides. The concentration of interstitial oxygen C_O in the samples amounted to $(9 \div 11) \times 10^{17}$ cm^{-3}, while that of carbon was equal to $\sim 2 \times 10^{16}$ cm^{-3}.

In order to form oxygen precipitates, we used the two-stage annealing during 20 h at 725 °C and during 5—20 h at 1050 °C in the atmosphere of pure argon. After that, the samples were treated in a ten-percent HF solution (10 min).

In order to determine the concentration of interstitial oxygen and oxygen precipitated to the SiO_2 phase in the investigated samples, we used the IR spectroscopy technique. Moreover, as a reference sample, we chose a silicon sample with a low content of oxygen (2×10^{15} cm^{-3}) obtained by means of the zone melting. The absorption band of valence vibrations of Si–O bonds (the maximum absorption is observed close to 1100 cm^{-1}) was measured with the help of a differential automatized IR spectrophotometer and a Fourier spectrometer. The optical density spectra were resolved into components of the Gaussian form. Moreover, for the absorption band associated with interstitial oxygen, the standard parameters (the position of the peak (1107±1) cm^{-1}, the half-width (33±1) cm^{-1}) were used [2]. The part of the absorption band left in the low-frequency spectral region is conditioned by the precipitated silicon-oxygen phase [1,2] and was described by a set of Gaussian profiles with the parameters characteristic of silicon-oxygen molecular clusters [5–7]. The accuracy of the deconvoluion was characterized by the standard deviation of the sum of Gaussian profiles from the experimental curve and didn't exceed 2×10^{-2} in the given work. The indicated parameters are presented in Table 1. The details of the method used for the determination of the structural state of oxygen in the silicon-oxygen phase and the analysis of the unambiguity of results of the mathematical

processing of spectral curves were described earlier [5–7].

The concentration of interstitial oxygen was determined by the intensity of the O elementary band using the coefficient of 3.03×10^{17} cm^{-3} [2]. The concentration of precipitated oxygen was estimated by the intensity of a low-frequency absorption band separated for the silicon-oxygen phase [7] in the mathematical processing of the spectrum (see the sum of $P1$–$P3$ profiles in Table 1).

A geometrical pattern of the structural network of the precipitated phase was obtained by the computer simulation on the basis of the analysis of the absorption band form. The clusters of the SiO_2 phase were constructed in the form of a mixture of the 4- and 6-membered rings of SiO_4 tetrahedra that included up to 150 silicon and oxygen atoms. The energy minimization was fulfilled based on the well-known semiempirical approach [8].

The data on the type, dimensions, and concentration of structural defects were obtained with the help of the techniques of X-ray diffraction and electron microscopy. In the first case, we used the measurements of the half-width of diffraction reflection curves (DFC) and the method of diffuse X-ray scattering (DXRS). We used $CuK_{\alpha1}$ radiation (the wavelength λ=0.15406 nm), the 004 symmetric reflections. The diffuse scattering and DFC were measured with the help of an "X'Pert PRO MRD" high-resolution X-ray diffractometer. The measurements were carried out close to the 004 site. The technique is described in works [9–12]. In addition to the determination of such microdefects as precipitates and those of a new phase, the DXRS technique allows one to discover the clusters of point defects that are coherent with the matrix and characterized with a diffuse interface and the low gradients of displacement fields and can't be discovered by electron microscopy. Apart from the detection of these microdefects, this technique allows one to recognize their type (vacancy or interstitial one), as the asymmetric part of DXRS shifts the scatterings from different types of defects to different sides from a site of the reciprocal lattice [11]. Thus, we can observe defects and classify them.

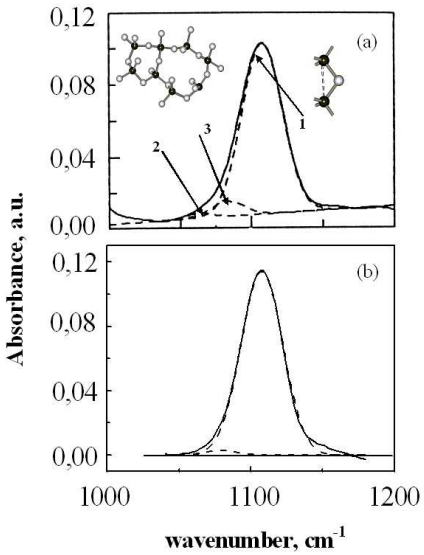

Fig. 1. Absorption band of Si–O bonds (solid curve) and its Gaussian components (dashed curves) for the initial Cz-Si samples 40 mm (*a*) and 300 mm (*b*) in diameter. *1* – interstitial oxygen; *2* – 4-membered rings of SiO_4 tetrahedra; *3* – 6-membered rings of SiO_4 tetrahedra

The additional information on the defect state of the crystal was obtained from the etching patterns (in a Sekko preferential etch) observed with the help of a HITACHI S-806 electron microscope.

The lifetime of nonequilibrium charge carriers τ was determined by a decrease of the nonstationary photoconduction under conditions of a low excitation level. The influence of attachment was eliminated due to the continuous lighting with white light. The measurement error didn't exceed 10%. The diffusion length of nonequilibrium charge carriers L was calculated using the measured values of τ according to the expression $L = \sqrt{D\tau}$, where the diffusion coefficient $D = 12$ cm^2/s for n-Si and $D = 36$ cm^2/s for p-Si.

3. Results and Their Discussion

Figure 1 shows an example of the decomposition of the optical density spectra of initial silicon plates. One can see from the figure that, for plates of large diameter (300 mm), the absorption band is mainly described by one

T a b l e 1. Characteristics of the elementary absorption bands

Band	Maximum position, cm^{-1}	Half-width, cm^{-1}	Bond angle Si–O–Si, degr.	Principal structural component
O	1107±1	33±1	162	interstitial oxygen
$P1$	1085±1	25±1	142	6-membered rings of SiO_4 tetrahedra
$P2$	1060±3	25±2	132	4-membered rings of SiO_4 tetrahedra
$P3$	1035±3	25±3	126	Si–O_2–Si_2 complexes

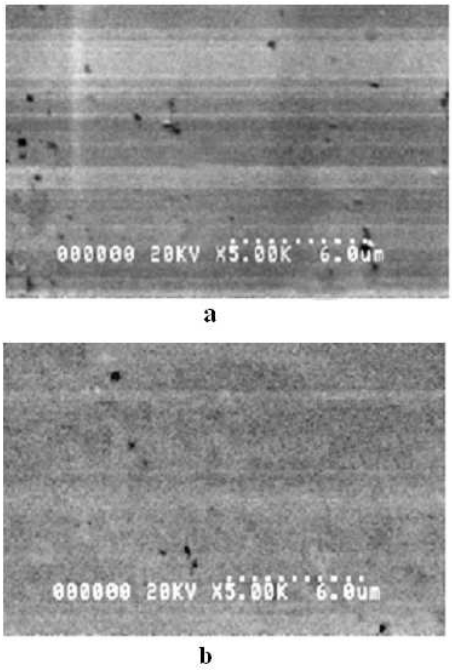

Fig. 2. Etching patterns of the initial Cz-Si samples 40 mm (*a*) and 300 mm (*b*) in diameter

Gaussian profile O, which testifies to the fact that the number of oxygen precipitates in such silicon is low. At the same time, the absorption band for silicon plates of small diameter (40, 76, and 100 mm) contains weak profiles $P1$ and $P2$ along with the principal one. Thus, these ingots include some amount of the precipitated oxygen phase that has created microclusters, whose structure can be presented as a mixture of the 4- and 6-membered rings of SiO_4 tetrahedra. The estimations of the concentration of precipitated oxygen in these samples give the value of the order of 5×10^{16} cm^{-3}. In other words, on growing Cz-Si crystals by the old technology, approximately 5% of oxygen in an ingot formed an inclusion of the silicon-oxygen phase, whose presence resulted in the appearance of mechanical stresses, which could cause, in turn, the inhomogeneous distribution of impurities (including the doping one) due to the effects of internal gettering, the appearance of point defects, etc.

Figure 2 demonstrates the etching patterns for two initial crystals: the samples cut out of ingots 40 mm (*a*) and 300 mm (*b*) in diameter. One can see that small etch pits are present in the both cases. The concentration and size are given in Table 2. One can conclude that the size of etch pits amounts to 0.05–0.1 μm, while their density in the samples with d=40 mm is essentially (by a factor of 4) larger than that in the samples with d=300. Judging by the size, these pits can be regarded as growth microdefects of the B-type (B-clusters). There exist several viewpoints concerning the nature of B-clusters. The most widespread model is the one, according to which B-clusters represent small dislocation loops of the vacancy or interstitial type [13, 14].

In Table 2, we also present the results of measurements of the lifetime and diffusion length of nonequilibrium charge carriers in the initial silicon samples. One can see that, in the samples with d=40 mm and d=300 mm, the magnitude of τ amounts to 6–8 and 20–23 μs, correspondingly. In other words, the lower the concentration of growth microdefects of small dimensions (B-type), the higher the lifetime of nonequilibrium charge carriers. This fact agrees well with the literature data. In particular, it is known that the presence of growth defects in Si results in a decrease of τ [15]. Moreover, the same as in our case, there takes place the correlation between the concentration of microdefects and the level of degradation of τ [15,16]. Thus, it is the low-dimension growth microdefects observed in the investigated samples that represent effective recombination centers.

Figure 3 shows the X-ray reflection curves for the 004 reflection of the initial plates. The values of the DFC half-widths obtained from them are given in Table 3. As one can see from the analysis of these data, the samples obtained from the 300-mm ingots have the minimal half-width. As the half-width of the reflection curve represents an integral characteristic of the structural perfection of a crystal, these samples can be regarded as the most perfect ones. It is worth noting that a half-width of 5 seconds of arc is very close to its theoretical value for the given reflection.

In order to investigate the nature and parameters of the defects in more details, we used the DXRS method. The results of studying the clusters of point microdefects are given in Fig. 4 showing the DXRS intensity

T a b l e 2. Defect and electrophysical characteristics of the Cz-Si initial samples

Ingot diameter, mm	Size of etching pits, μm	Density of etching pits, cm^{-2}	Lifetime, μs	Diffusion length, μm
40	0.05–0.1	$\sim2\times10^7$	6–8	85–90
300	0.05–0.1	$\sim5\times10^6$	20–23	265–270

T a b l e 3. Diffraction and structural parameters of the initial Cz-Si samples

Ingot diameter, mm	Half-width, sec. of arc	Size of microdefects of vacancy type, μm	Size of microdefects of interstitial type, μm
40	7.8	0.289	0.278
300	5.6	0.220	0.285

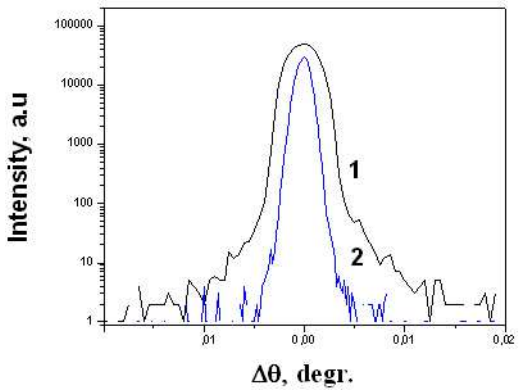

Fig. 3. Diffraction reflection curves for the 004 reflection for the initial Cz-Si samples 40 mm (*a*) and 300 mm (*b*) in diameter

distribution along the direction normal to the reciprocal lattice vector (q_x cross section) and parallel to it (q_z cross section), where the q-vector denotes the distance from the reciprocal lattice site to the point, in which the intensity is measured. Analyzing the DXRS intensity distribution $I(q)$ for all the samples, one can note that they include microdefects of both the vacancy type (to which the intensity at $q_z < 0$ corresponds) and the interstitial one ($q_z > 0$). From Fig. 4,*b*, one can conclude that the magnitude of the presented intensity $I(q)q^3$ is practically constant in the whole range of q_z values. This fact implies that the scattering takes place in the asymptotic scattering region, where the power of the defect C is proportional to $q_g g(QC)^{-1/2}$ [10], where Q is the scattering vector. The point of transition to the horizontal region of these dependences allows one to determine the dimensions of microdefects, whose values are also presented in Table 3.

The scattering intensity at negative values of q_z is somewhat larger and, consequently, the total volume of vacancy defects is distinctly larger (approximately by a factor of two) than that of interstitial ones, as the intensity is proportional to the volume of defects. The behavior of the intensity at the q_x cross section for the Si sample 300 mm in diameter testifies that the displacement fields of the defects present in it are characterized by a symmetry close to the spherical one. A somewhat higher intensity at the q_x cross section (Fig. 4,*b*) for 40-mm samples allows one to conclude that, among the microdefects, these exist ones with a nonspherical symmetry of displacement fields.

The first stage of the annealing (725 °C, 20 h) changed weakly the concentration of interstitial oxygen and resulted in some growth of the content of the oxide

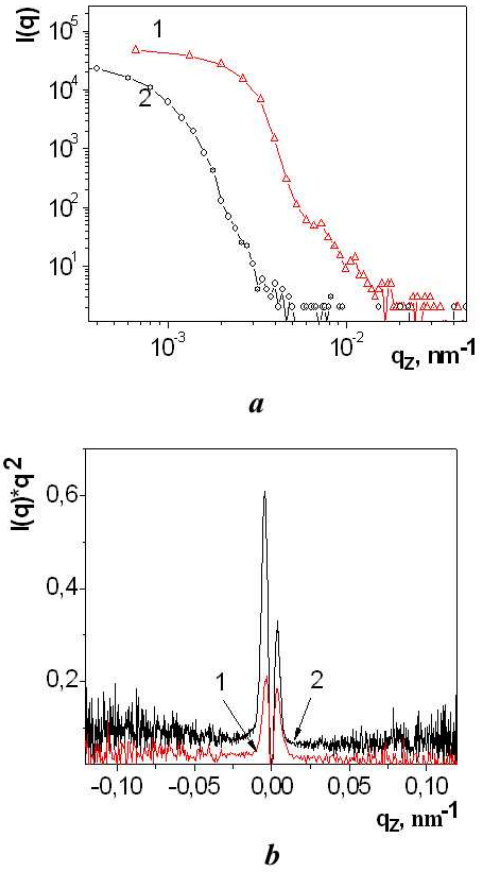

Fig. 4. Intensity distribution of the diffraction scattering along the q_x cross section (*a*) and q_z cross section (*b*) of the reciprocal space of the 004 site for 40-mm (*1*) and 300-mm (*2*) initial Cz-Si samples

phase (possibly the nuclei of prospective developed oxygen precipitates) in all the investigated samples. The structure of this phase depends on the type of a sample. For example, in ingots of small diameters, the annealing results in the essential growth of the concentration of oxygen atoms that form the 4-membered rings of SiO_4 tetrahedra. In contrast, the samples cut out of large-diameter ingots (300 mm) are characterized by the appearance of an only weakly stressed precipitated phase, whose lattice includes only the 6-membered rings of SiO_4 tetrahedra. The concentration of oxygen atoms that have formed this phase in samples of such a kind during the first stage of the annealing amounts to the value of the order of 4×10^{16} cm^{-3}, that is, it is practically the same as that in the initial small-diameter ingots.

The high-temperature (1050 °C) stage of the thermal treatment essentially decreases the concentration of interstitial oxygen in all the samples (Fig. 5). In this

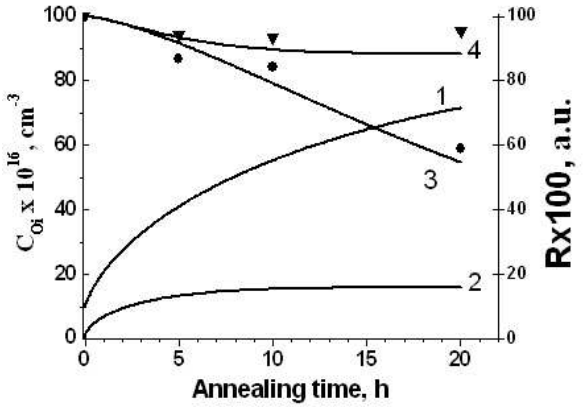

Fig. 5. Experimental dependences of the concentration of interstitial oxygen on the duration of the 1050 °C annealing for 300-mm (dots) and 40-mm samples and the simulation results of the release kinetics of interstitial oxygen (*3*, *4*) and the change in the precipitates dimensions (*1*, *2*) during the high-temperature stage of the annealing of 40-mm (*1*, *3*) and 300-mm (*2*, *4*) silicon plates

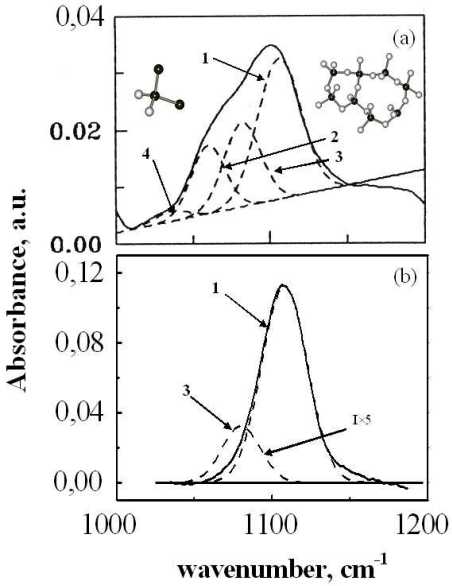

Fig. 6. Absorption band of Si–O bonds (solid curve) and Gaussian components (dashed one) of 40-mm (*a*) and 300-mm (*b*) Cz-Si samples annealed during 20 h at 1050 °C: *1* — interstitial curves; *2* – 4-membered rings of SiO_4 tetrahedra; *3* – 6-membered rings of SiO_4 tetrahedra; *4* – $Si–O_2–Si_2$ complexes

case, the concentration of O_i in small-diameter ingots decreases almost by a factor of two (by 75%) after the 20-h annealing, as these ingots are more liable to the influence of temperature. In large-diameter ingots, the indicated effect is weaker (10%).

The technology of silicon production also affects essentially the processes of precipitation of oxygen during the high-temperature stage of the annealing (Fig. 6). In the case of low-diameter ingots, the concentration of precipitated oxygen atoms essentially increases and reaches 3.6×10^{17} cm^{-3} after the 20-h annealing. In this case, along with the growth of P1 and P2 components, these appears a new component P3 in the absorption spectrum, which is associated with $Si–O_2–Si_2$ molecular complexes. It's not inconceivable that the indicated complexes exist in the silicon lattice independently. However, our recent investigations of "silicon — thin (10–15 nm) thermal oxide" systems performed with the help of IR-spectroscopy and spectral ellipsometry [17] have demonstrated the existence of such complexes in the structure of a $Si–SiO_2$ transient layer. One can assume that, in the case of the formation of the developed inclusions of oxygen precipitates in Cz-Si, $Si–O_2–Si_2$ complexes are also most likely localized close to the silicon-precipitate interface.

In large-diameter ingots, the high-temperature stage of the annealing practically didn't result in a change of the content of precipitated oxygen atoms or the molecular structure of the precipitated oxide phase.

Figure 7,*a* shows the results of a computer simulation of the structural network of silicon dioxide that consists only of 6-membered rings (large-diameter ingots). In this case, we can say about the formation of a quite ordered structure which is, most likely, similar to the low-temperature phase of α- cristobalite [18]. The simulated structure of the precipitated phase in the case of low-diameter ingots is depicted in Fig. 7,*b*.

Summing up what was said above, we can mark out two fundamentally important points:

1. Low-diameter ingots are characterized by the presence of a high content of small (0.05—0.10 μm) growth microdefects that represent small dislocation loops of the vacancy type. These defects are electrically active, and their presence results in the degradation of the lifetime and the diffusion length of nonequilibrium charge carriers.

2. In the samples obtained from low-diameter ingots, the process of oxygen precipitation at high temperatures is characterized by a high intensity; it results in the formation of SiO_2 regions, whose structure is characterized by the essential content of the stressed 4-membered rings of SiO_4 tetrahedra. These regions are surrounded by layers that contain not completely oxidized silicon (for example in the form of $Si–O_2–Si_2$) molecular clusters).

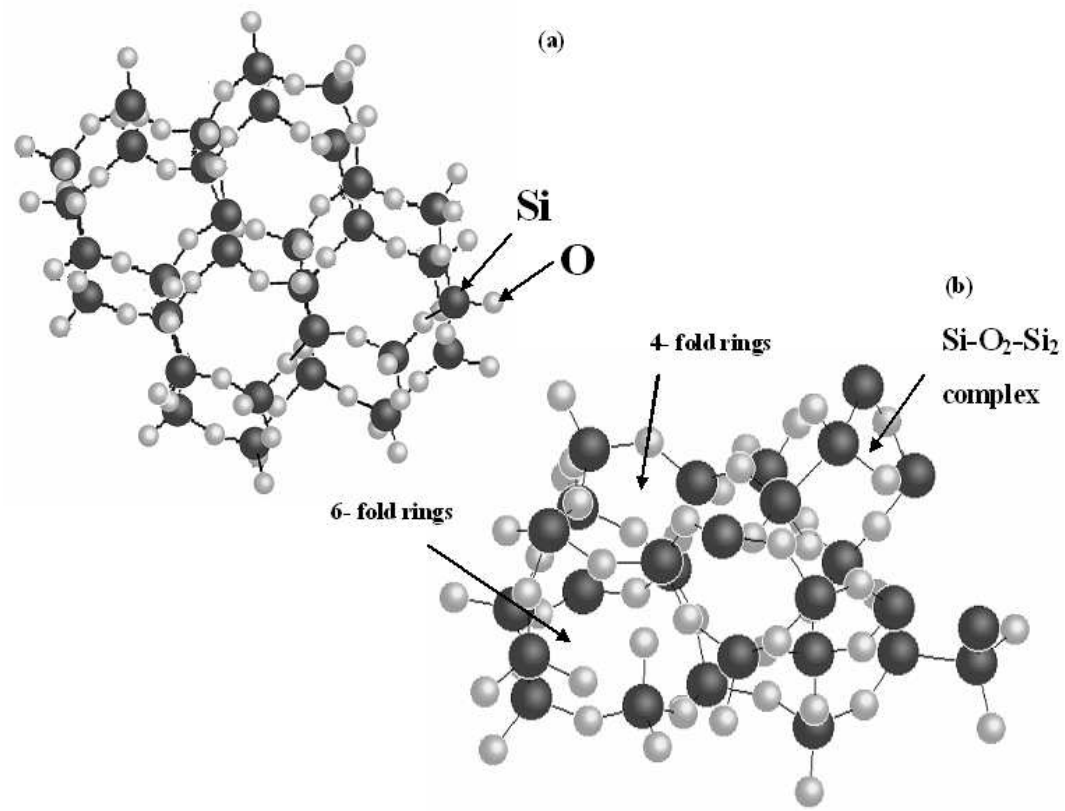

Fig. 7. Structural network of oxygen precipitates in the large-(a) and low-diameter (b) annealed samples 6-membered ring 4-membered ring complex

It is known that the rates of growth and cooling of low-diameter silicon crystals are higher than those of large-diameter ones [13]. This fact must cause the appearance of a larger number of growth defects in low-diameter ingots, which is confirmed by the measurements of the density of microdefects and electrophysical characteristics of samples. A long-term thermal treatment at 725 °C raises the content of microdefects in plates proportionally to their initial concentrations. That is, the contrast between ingots of small and large diameters still increases. A high density of microdefects must give rise to the appearance of the relatively intense fields of mechanical stresses in such samples (as compared to the situation in large-diameter ingots). During the high-temperature (1050 °C) stage of anneal, silicon is rather plastic. But, in the process of cooling of the samples, the indicated stresses must stimulate the formation of the strongly stressed precipitated oxide phase in low-diameter ingots, whose structural network contains the deformed 4-membered rings of SiO_4 tetrahedra.

Let us consider the kinetics of the high-temperature stage of the annealing (Fig. 5) in more details. It should be taken into account that, in the initial stage, both types of the samples contain practically the same number of atomic oxygen bound in interstitial sites, but essentially different concentrations of microdefects. If we assume the absence of other sinks for oxygen except those that already have been formed at the structural defects of nuclei of the SiO_2 phase, the simplest equations of mass balance for mobile (released) interstitial (C_i) and bound (C_p) oxygen can be presented as

$$dC_i/dt = -dC_p/dt = k_{i\to b}(C_i - C_{\rm if})N_p, \qquad (1)$$

$$dR^2/dt = 2D(C_i - C_{\rm if})/(C_{\rm pr} - C_{\rm if}), \qquad (2)$$

where $k_{i\to b}= 4\pi DR$ stands for the rate constant of the diffusion-limited growth/decay of a precipitate of radius R; D is the diffusion coefficient, $C_{\rm pr}$ denotes the oxygen concentration in the SiO_2 phase, C_i is the current concentration of interstitial oxygen in silicon, N_p is the

number of precipitates in the unit volume of the matrix, while $C_{\rm if}$ represents the equilibrium concentration of the mobile oxygen close to the curved SiO_2/Si interface. With allowance for the Gibbs–Thomson effect, the latter quantity can be presented as

$$C_{\rm if} = C_{\rm eq} \exp(2\gamma\Omega/Rk_{\rm B}T) \approx C_{\rm eq}(1 + 2\gamma\Omega/Rk_{\rm B}T), \quad (3)$$

where γ denotes the specific free energy of the interface, Ω is the atomic volume of oxygen in the new phase, T is the annealing temperature, $C_{\rm eq}$ denotes the equilibrium solubility of oxygen in silicon at a given temperature, and $k_{\rm B}$ is the Boltzmann constant. One can see that the contribution of curvature is evidently essential for the first stage of the "ripening" of nuclei and relatively small for rather high temperatures characteristic of the second stage of the annealing. However, it is worth taking into account (as follows from the Van Hellemont–Clayes formula [19] for the critical radius R_c) the fact that, in our case, the nucleation and the phase growth depend on the presence of point defects of both signs. This point will be accounted for in the simplest variant considering that growth ($C_{\rm if} < C_i$) takes place if $R > R_c$. Moreover, the more the surrounding of the precipitate is saturated with excess vacancies, the lower R_c. In addition, we don't take into account, in this stage, the decay of subcritical nuclei ($C_{\rm if} > C_i$, $R < R_c$) considering that this faster process occurs in the very initial stage of the annealing and is not fixed on the experimental kinetic curve.

Thus, we will consider in what follows that the system consists of identical subcritical nuclei of radius R with the concentration of N_p surrounded with interstitial oxygen with the concentration of C_i, while the interface concentration $C_{\rm if}$ is considered as a free parameter which reflects qualitatively the defect status of a sample and should be determined.

According to (1), a faster loss of interstitial oxygen observed for the low-diameter ingots can be conditioned by the following reason. Since we observed no deceleration of the kinetics even after the 20-h annealing for the low-diameter ingots, we can conclude that the concentration $C_{\rm if}$ is rather low in this case. This fact can be explained by the presence of vacancy-enriched atmospheres close to the SiO_2/Si interface or the presence of a transient layer of the SiO_x type enriched with intermediate $Si—Si_2—O_2$ complexes that manifest themselves in IR spectra. In both cases, any excess oxygen atom in the silicon matrix, that appears in the surrounding of the precipitate, will be actively absorbed by the interface zone maintaining a high level of the diffusion-driven delivery.

For the large-diameter samples, it is evident that the process of high-temperature precipitation completely ends by the tenth hour of the annealing. This fact can be explained by a high value of $C_{\rm if}$ in connection with a high rate of oxygen absorption. At the end of the annealing, the silicon matrix of the given type contains precipitates surrounded with a rather dense atmosphere of untrapped excess oxygen. Thus, we can state that, in a certain stage, the oversaturation with oxygen becomes insufficient for the further growth of precipitates. For example, it can take place due to the insufficient generation of excess vacancies, which is characteristic of SiO_2 precipitates with a surplus of free volume. Being more prone to external deformations, they can easily relax in the process of accommodation in the silicon matrix due to a decrease of the own volume, rather than to the generation of additional silicon vacancies. Such a mechanism agrees well with the IR spectroscopy data on the structural state of precipitated oxygen (freer 6-membered rings) in plates of large diameter.

It is worth noting that the total absorption capacity of precipitates is proportional to DN_p, whereas the total number of bound oxygen is proportional to N_p^3. That's why, comparing the calculated kinetic curves, we will deal with relative magnitudes of the radius choosing N_p as a parameter. At the same time, the value of N_p^3 can be determined experimentally considering that a decrease of interstitial oxygen corresponds to the increase of oxygen bound in precipitates. This allows one to compare the data for both types of the samples dealing with the relative quantities R and N_p.

In Fig. 5, the kinetics of a decrease in the oxygen concentration and an increase in the average radius of a precipitate calculated for plates of different types is compared with the experimental data. The parameters of calculations allowing one to reach a good agreement between theory and experiment are given in Table 4. The notations used in Table 4 are as follows: C_0 and C_f are, respectively, the initial and final concentrations of interstitial oxygen; R_0 and R_f are the initial and final (averaged) radii of precipitates; P_0 and P_f are the initial

T a b l e 4. Parameters of the calculation for the curves given in Fig. 5

Sample	$C_0 \times 10^{16}$, cm^{-3}	$C_f \times 10^{16}$, cm^{-3}	R_0, arb.un.	R_f, arb. un.	P_0, arb. un.	P_f, arb. un.	ΔC	ΔP
300 mm	100	88.1058	0.001	0.1607	0.0000	11.8942	11.8942	11.8942
40 mm	100	54.7592	0.1	0.7144	0.1244	45.3652	45.2408	45.2408

and final concentrations of bound oxygen. In the calculations, we assumed that the initial radii of the nuclei relate as R_{40}/R_{300}=0.1/0.001 (hereinafter, the indices correspond to the diameters of ingots). The concentrations of the precipitates are set as N_{p300}/N_{p40}=25. The equilibrium concentration of oxygen at the SiO_2/Si interface is directly determined from the experiment, and C_{if300}/C_{if40} ∼9. This agrees well with the conception of stability of low-diameter precipitates in the presence of a rather dense atmosphere of atomic oxygen around them, which prevents them from the decay.

The results obtained from the calculations allow us to make a number of fundamental conclusions:
– the large-diameter plates are characterized by the presence of a large number of precipitates of a very low size that are well bound with the silicon matrix (the final radii of the precipitates relate approximately as 1:5);
– the quantity of bound oxygen in such samples after the annealing is lower than that in the low-diameter plates approximately by a factor of 4;
– from the viewpoint of the creation of an internal getter, precipitates in the large-diameter plates are more effective approximately by a factor of 5 as compared to ones in the low-diameter plates.

4. Conclusions

We have shown that the precipitated oxygen phase in low-diameter ingots is characterized by the presence of a rather stressed configuration of the rings of SiO_4 tetrahedra. A facilitated decay of the latter is one of the reasons for the thermal relaxation of mechanical stresses as well as the thermal instability and instabilities of the other types. In contrast, the large-diameter material contains a relatively low concentration of electrically active growth microdefects which are small (0.06–0.1 μm) dislocation loops. We consider that just this circumstance results in a higher stability of such a silicon during thermal treatments and in the formation of the weakly stressed oxide phase (SiO_2) which doesn't include the strongly deformed rings of SiO_4 tetrahedra.

The component of IR-spectra at ∼1085 cm^{-1}, which is associated with valence vibrations of oxygen atoms in the structure of the 6-membered rings of SiO_4 tetrahedra, can be considered as an evidence for the stability of the Si-matrix, while its intensity relative to the other components – as a measure of the stability in the proposed nondestructive method of analysis of the Cz-Si material.

1. K. Tempelhoff, F. Spiegelberg, R. Gleichmann, and D. Wruck, Phys. Stat. Sol. (a) **56**, 213 (1979).
2. B. Pajot, H.J. Stein, B. Cales, and C. Naud, J. Electrochem. Soc. **132**, 3034 (1985).
3. K. Nakai, Y. Inoue, H. Yokota *et al.*, J. Appl. Phys. **89**, 4301 (2001).
4. A.A. Efremov, V.G. Litovchenko, A.V. Saricov, H. Richter, and V. Akhmetov, Solid St. Phenom. **95–96**, 405 (2004).
5. I.P. Lisovskyy, V.G. Litovchenko, V.B. Lozinskii *et al.*, Thin Solid Films **213**, 164 (1992).
6. I.P. Lisovskyy, V.G. Litovchenko, V.B. Lozinskii *et al.*, J. Non-Cryst. Solids **187**, 91 (1995).
7. I.P. Lisovskyy, Ukr. Fiz. Zh. **42**, 1260 (1997).
8. J.G. Vinter, A. Davis, and M.R. Saunders, J.Comput.-Aided Mol. Des. **1**, 31 (1987).
9. V.T. Bublik and K.D. Shcherbachev, Kristallogr. **42**, 326 (1997).
10. M.A. Krivoglaz, *Diffraction of X-Rays and Thermal Neutrons in Imperfect Crystals* (Naukova Dumka, Kyiv, 1983) (in Ukrainian).
11. V.T. Bublik and K.D. Shcherbachev, Kristallogr. **39**, 1105 (1994).
12. V.P. Kladko, L.I. Datsenko, J. Bak-Misiuk, S.I. Olikhovskii, V.F. Machulin, I.V. Prokopenko, V.B. Molodkin, and Z.V. Maksimenko, J. Phys. D: Appl. Phys. **34**, A87 (2001).
13. K.V. Ravi, *Imperfections and Impurities in Semiconductor Silicon* (Wiley, New York, 1981).
14. V.G. Litovchenko, Polupr. Tekhn. Elektr. 3 (1981).
15. A. Usami, K. Okura, and T. Maki, J. Phys. D: Appl. Phys. **10**, L63 (1977).
16. I.M. Gres'kov, B.V. Smirnov, S.P. Solov'ev *et al.*, Fiz. Tekhn. Polupr. **12**, 1879 (1978).
17. A. Szekeres, A. Paneva, S. Alexandrova, I. Lisovskyy, V.G. Litovchenko, and D. Mazunov, Vacuum **69**, 355 (2003).
18. A.G. Revesz, Phys. Status Solidi **57**, 235 (1980).
19. J. Van Hellemont and C. Clayes, J. Appl. Phys. **62**, 3960 (1987).

Received 12.03.07.
Translated from Ukrainian by H.G. Kalyuzhna

ВПЛИВ ДЕФЕКТІВ НА СТРУКТУРУ КИСНЕВИХ ПРЕЦИПІТАТІВ В КРИСТАЛАХ КРЕМНІЮ

В.Г. Литовченко, І.П. Лісовський, В.П. Кладько С.О. Злобін, М.В. Муравська, А.А. Єфремов, М.В. Слободян

Р е з ю м е

Методами ІЧ-спектроскопії з комп'ютерним аналізом форми смуги поглинання, електронної мікроскопії, дифракції рентгенівських променів та вимірювання спаду нестаціонарної фотопровідності в умовах низького рівня збудження проведено експериментальне дослідження впливу дефектів у кремнієвих

зливках різного діаметра (40 – 300 мм) на процеси утворення кисневих преципітатів у процесі двостадійного відпалу (750 та 1050 °C). Для досліджень використано монокристали кремнію, вирощені методом Чохральського (Cz-Si). Показано, що у зразках великого діаметра містяться з відносно низькою концентрацією електрично активні мікродефекти, які являють собою малі (0,06 – 0,1 мкм) дислокаційні петлі. Ця обставина приводить до формування в результаті термообробок слабконапруженої фази окислу SiO_2, що не містить деформованих 4-членних кілець тетраедрів SiO_4 (характерних для преципітатної кремній-кисневої фази у зливках малого діаметра), і, як наслідок, до підвищеної термостабільності такого кремнію.